Journal of South American Earth Sciences 32 (2011) 142–151

Contents lists available at ScienceDirect

Journal of South American Earth Sciences

journal homepage: www.elsevier.com/locate/jsames

Basement depths in the Parecis Basin (Amazon) with receiver functions from small local earthquakes in the Porto dos Gaúchos seismic zone

Lucas Vieira Barros [a,*], Marcelo Assumpção [b]

[a] Seismological Observatory, University of Brasilia, Brasília DF 70910-900, Brazil
[b] Institute of Astronomy, Geophysics and Atmospheric Sciences, University of São Paulo, São Paulo, SP 05508-090, Brazil

ARTICLE INFO

Article history:
Received 7 October 2009
Accepted 7 April 2011

Keywords:
Amazonian craton
Intraplate seismicity
Parecis basin
Receiver function

ABSTRACT

Receiver functions from small local earthquakes were used to determine sediment thicknesses in Porto dos Gaúchos seismic zone (PGSZ), Parecis basin, Amazonian craton, Brazil. The high velocity contrast between basement and sediments (P-wave velocities of 6.1 and 3.0 km/s, respectively) favors the generation of clear P-to-S converted phases (Ps) seen in the radial component, and also S-to-P conversions (Sp) seen in the vertical component. A reference 1D velocity model determined with shallow refraction experiment in PGSZ helped to convert Ps–P time differences to basement depths at 15 stations deployed for aftershocks studies. The results of receiver function integrated with the shallow refraction reveal that the basement depths in the PGSZ increases from the basin border in the north up to about 600 m depth in the south.

The basement topography, however, does not vary smoothly and a basement high with a steep topography was detected near the epicentral area. A 400 m elevation difference within 1.7 km distance suggests a possible border fault of a buried graben. This feature seems to be oriented roughly WSW-ENE and could indicate basement structures related to the seismicity of the Porto dos Gaúchos Seismic Zone.

1. Introduction

The Parecis basin is located in central-west Brazil and covers the center north of Mato Grosso State and the eastern part of Rondônia State. Together with the Amazon and Paraná basins (Fig. 1, inset) define the set of the Brazilian Paleozoic intracratonic basins adjacent to the sub-Andean depression. The stratigraphic column includes Paleozoic, Mesozoic and Cenozoic units, whose development was under strong tectonic influence of the past margins of the South American continent (Siqueira, 1989). The main depocenters are located in its central part (Pimenta Bueno graben) and in its northern part (NW Xingu and Caiabis grabens), where, according to Braga and Siqueira (1996), depths could reach up to 9.5 km (Fig. 1).

The largest earthquake ever observed in the stable continental interior of the South American plate (large circle in Fig. 1) occurred on January 31, 1955, in the Parecis basin with a magnitude of 6.2 m_b. Since then, no other earthquake has been located in the area of the 1955 event. However, in Porto dos Gaúchos, 100 km NE of the 1955 epicenter, a recurrent seismicity has been observed since 1959, two years after the arrival of the first inhabitants in the region (Barros et al., 2009). Two magnitude 5 earthquakes have occurred in Porto dos Gaúchos, one in 1998 and the other in 2005, with aftershock sequences lasting for more than four years each. These two aftershock sequences were studied with local seismographic networks (Barros et al., 2011; Barros et al., 2009; Barros, 2010). This active area of the Parecis basin has been called the Porto do Gaúchos Seismic Zone (PGSZ).

The PGSZ (Figs. 1 and 2) includes Phanerozoic rocks of the Parecis basin and Precambrian rocks of the Amazonian craton (southern part of the Rio Negro-Juruena geochronologic province), in addition to the Caiabis graben of Mesoproterozoic age (~1.36 Ga) (Tassinari et al., 2000; Leite and Saes, 2003). Basement depths in the PGSZ are not well known. Fig. 1 shows the basement topography of the Parecis basin estimated from regional 3D gravity modeling by Braga and Siqueira (1996). This model was constrained by sparse seismic and well data located mainly in the southern and western parts of the basin, such as the Pimenta Bueno graben, far from the study area of Porto dos Gaúchos (Fig. 2).

Seismograms of the local earthquakes recorded clear Ps (P converted to S) and Sp (S converted to P) phases from the basement–sediment interface. The Ps–P time difference can be used to estimate the sediment thickness under each station, since this difference is proportional to the depth of the discontinuity that causes the converted Ps phase. In addition, a seismic refraction

* Corresponding author. Tel.: +55 61 9981 0604; fax: +55 61 3274 5927.
E-mail addresses: lucas@unb.br (L.V. Barros), marcelo@iag.usp.br (M. Assumpção).

0895-9811/$ – see front matter © 2011 Elsevier Ltd. All rights reserved.
doi:10.1016/j.jsames.2011.04.002

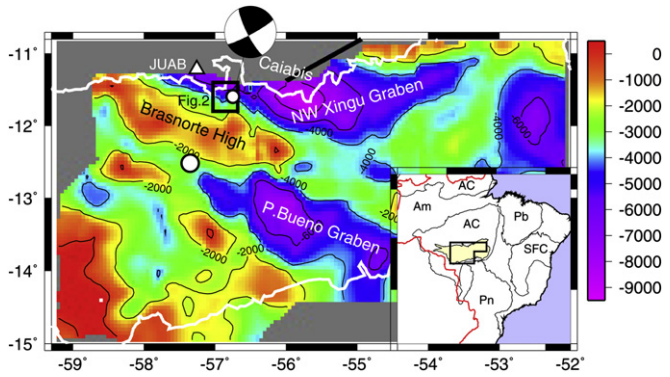

Fig. 1. Contour map of gravity-derived basement depths (m) of the Parecis Basin and interpreted major structural boundaries (modified from Braga and Siqueira, 1996). The solid square shows the study area (Fig. 2) with the small open circle denoting the epicenter of the 1998/2005 earthquakes. The large open circle is the epicenter of the 1955 earthquake. The triangle is JUAB station in the exposed basement of the Amazonian craton. The focal mechanism solution is for the 2005 earthquake (Barros et al., 2009). Thick white line is the limit of the Parecis basin. The inset shows the main structural provinces in Brazil (Almeida et al., 2000): AC Amazonian craton; Am Amazon Basin; Pb Parnaiba Basin; Pn Paraná Basin; SFC São Francisco Craton. Red line is Brazil border. (For interpretation of the references to colour in this figure legend, the reader is referred to the web version of this article).

experiment was carried out using two explosions as active sources to determine the seismic velocities of the sedimentary layer and the basement. Thus the estimated velocity model was used to convert Ps–P times into sediment thickness. This study aims to map basement depths in the Porto dos Gaúchos Seismic Zone by integrating the shallow seismic refraction experiment with analyses of the Ps phase, using the receiver function technique at 15 seismic stations.

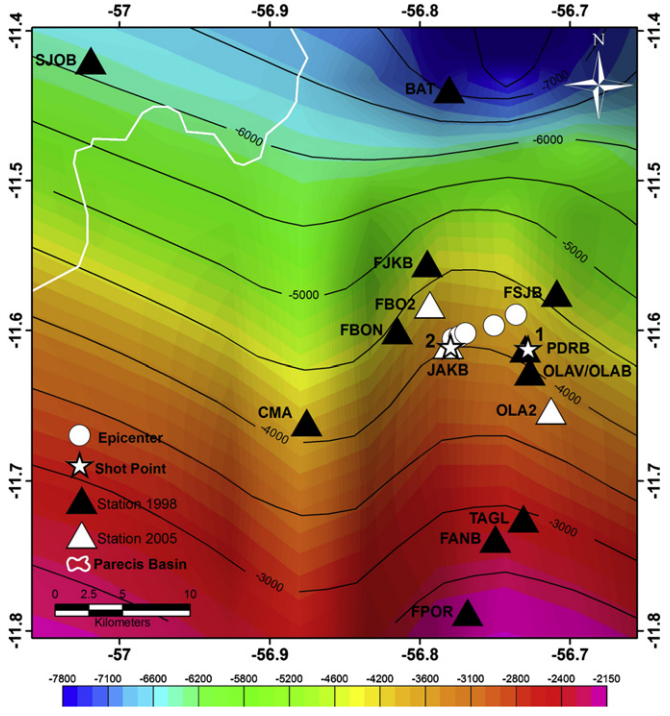

Fig. 2. Contour map of gravity-derived basement depths (color scale and contours in meters) in the study area from Braga and Siqueira (1996). Black and white triangles indicate, respectively, the stations of the 1998–2002 and 2005 deployments. FSJB station belongs to both deployments. The shot points are indicated by stars 1 and 2 and the circles are the best –located five epicenters of 2005 sequence. Map coordinates in degrees. (For interpretation of the references to colour in this figure legend, the reader is referred to the web version of this article).

2. Porto dos Gaúchos seismic zone

The seismicity of Porto dos Gaúchos is not well known. The first seismographic stations in the Amazon region were installed only in the beginning of 1980's. Since then, earthquakes of magnitudes between 3.5 and 4.4 m_b started to be detected. In March of 1998 and March of 2005, the two largest earthquakes in the seismic area of Porto dos Gaúchos were recorded: 5.2 m_b and maximum Modified Mercalli (MM) intensity VI, and 5.0 m_b and maximum intensity V (MM), respectively. Their aftershocks were studied with two University of Brasília (UnB) local seismographic networks (Barros et al., 2009, Barros et al., 2011). The first network of 10 stations (not all operating simultaneously) had an approximate diameter of 70 km and recorded over 2500 microearthquakes between March 1998 and December 2002. The second network used five stations in an area with a diameter of about 12 km and recorded over 3500 microearthquakes in a period of six months. Broadband (30 s – 50 Hz) and short period (1 Hz – 100 Hz) sensors were used with 100 samples per second. Fig. 2 shows the station locations of both networks, the five best-located epicenters of the 2005 seismic sequence and the two shot points of the refraction experiment. JUAB station, of the 1998–2002 network, is shown in Fig. 1. The basement topography contours shown in Fig. 2 were estimated by Braga and Siqueira (1996) with 3D modeling of regional gravity. However, there are no independent depth controls near our study area, so that the estimated depths have no local meaning, except to indicate a trend of lower gravity toward the Xingu and Caiabis graben systems in the north.

Hypocentral locations were estimated using a 1D P-wave velocity model from the seismic refraction, with Vp/Vs ratio of 1.71 (obtained with a Wadati diagram) for the 1998 sequence and 1.78 for the 2005 sequence (Barros and Caixeta, 2003; Barros et al., 2009). These differences in the average Vp/Vs ratios are due to the different network apertures: more distant stations record waves traveling predominantly in the granitic/gneissic basement (lower Vp/Vs), while the ray paths to nearby stations sample predominantly the sediments (higher Vp/Vs). Both the 1998 and 2005 earthquake sequences occurred in the same WSW-ENE oriented fault zone with right-lateral strike-slip motion. The epicentral zone is located near a basement high, SW of the deep Mesoproterozoic Caiabis graben, which lies partially beneath the Parecis basin. However, the epicentral distribution is perpendicular to the trend of the Caiabis graben and so cannot be directly related with the Caiabis graben. It seems to be related to a N60°E trending fault (as mapped by Leite and Saes, 2003), which probably crosses the entire Caiabis graben, as proposed by Barros et al. (2009).

3. Ps and Sp converted phases

Fig. 3 shows the seismograms for two events, one recorded at station CMA (Fig. 3a) and the other at FJKB (Fig. 3b), where the converted Ps and Sp phases are very clear. In both cases, the P wave has large amplitude in the vertical component with the amplitude of the horizontal-radial component being very small. The radial/vertical amplitude ratio indicates a P wave arriving at the surface with a steep incidence angle of less than 10°.

The Ps phase, on the other hand, has larger amplitude in the radial component because it arrives at the station polarized as an SV wave with a steep incidence angle. The precursor to the S wave, identified in Fig. 3 as "Sp" phase, has larger amplitude in the vertical component because it arrives at the surface as a steep P wave. Fig. 4 shows a schematic ray diagram to explain the phase conversions and relative amplitudes of the P, Sp, Ps and S phases that would be observed in a uniform layer in the vertical (Z) and radial (R) components. Note that for an S-to-P conversion to occur, the

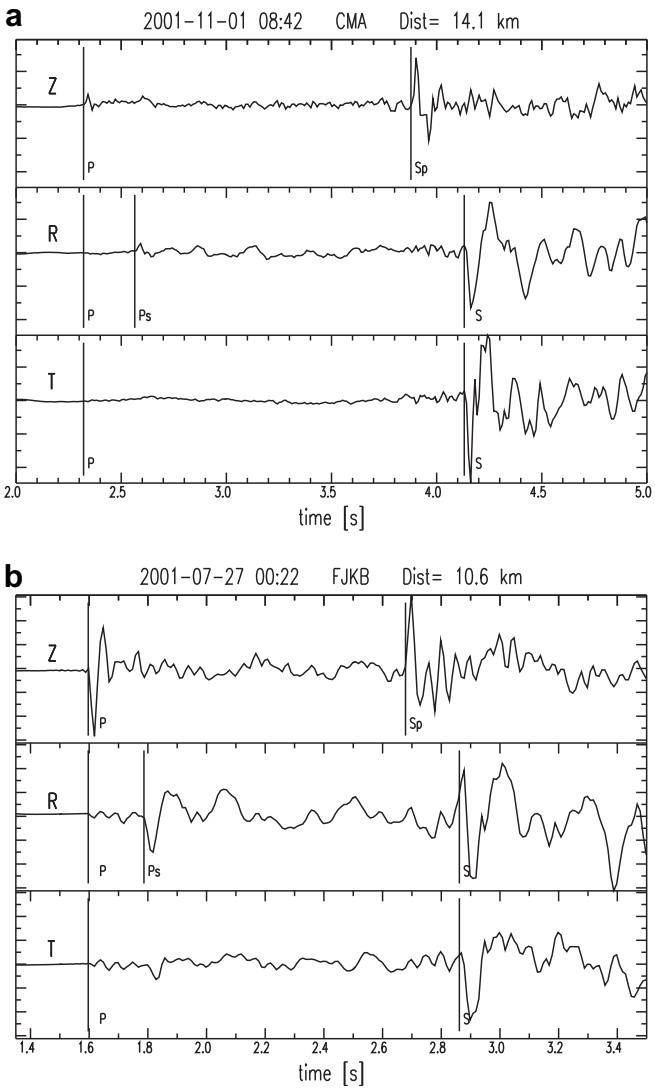

Fig. 3. Observed seismograms showing clear P-to-S converted phase (Ps) in the radial component and S-to-P (Sp) in the vertical component. Z, R and T denote the radial, transverse and vertical components, respectively. Same vertical scale for all three components. a) Event 22 (Table 1) at the station CMA (see location in Fig. 2). b) Event 18 (Table 1) at the station FJKB.

P-wave velocity of the sedimentary layer (α_1) must be lower than the S-wave velocity of the basement (β_2) as indicated in Fig. 4.

The Ps–P time (difference between the travel times of the converted Ps and the direct P phase) is similar to the S–Sp time; this is expected for 1D isotropic structures and confirms the identification of the Ps and Sp phases in all stations, such as shown in Fig. 3.

Because the direct P wave arrives at the station in a steep angle, the vertical component is, to a first approximation, similar to the P waveform incident at the basement/sediment interface. For this reason, a deconvolution of the vertical from the radial component gives a trace that can be interpreted, as a first approximation, to what would be recorded in the radial for a short pulse incident at the base of the layer with angle i_o. This is shown as a Receiver Function trace (RF) in Fig. 4c, as will be discussed in the next section.

The expression for the layer thickness, H, in terms of Ps–P can be derived based in Figs. 4 and 5. This will be used later in the combined interpretation of the refraction experiment with the Ps–P times. The

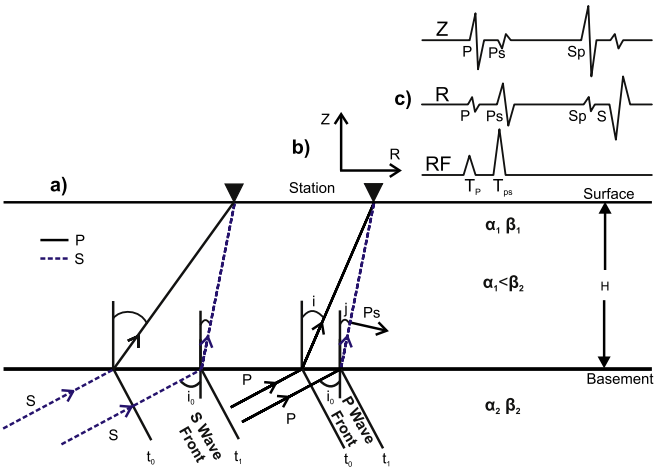

Fig. 4. Schematic ray diagram (a), Z and R component orientation (b), and relative amplitudes (c) of the P, Ps, Sp and S phases that would be observed in a uniform layer in the vertical (Z) and radial (R) components as well as the calculated radial receiver function (RF). α_1 and β_1 are the P- and S-velocities of the layer, α_2 and β_2 of the half-space.

difference between the Ps travel time (T_{Ps}) and the P time (T_P) is given by

$$T_{Ps} - T_P = (H/\cos j)/\beta_1 + \Delta T - (H/\cos i)/\alpha_1 \quad (1)$$

where H is the layer thickness; i and j are the surface incidence angles of the P and Ps phases, respectively; α_1 and β_1 are the layer P- and S-wave velocities, respectively; and ΔT is the time the P-wave front takes to sweep the distance ΔX with apparent velocity V_{AP} (Fig. 5). ΔX is the difference between the P and Ps offsets (X_P is the P offset and X_S is the Ps offset) and is given by

$$\Delta X = X_P - X_S = H(\tan i - \tan j) \quad (2)$$

or, in terms of the apparent velocity (V_{AP})

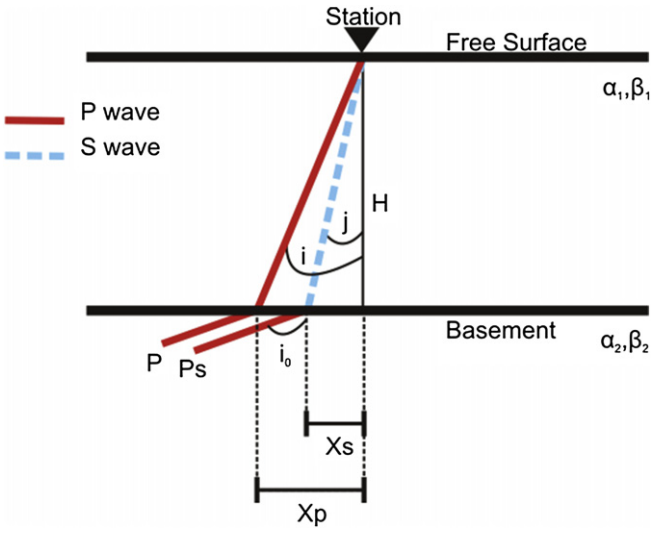

Fig. 5. Ray diagram for the direct P and converted phase Ps for a flat layer with thickness H over a half-space. i and j are the surface incidence angles of the direct P and converted phase Ps, respectively. I_o is the incidence angle of the P wave in the half-space. Xp and Xs are the offsets of the P and Ps, respectively. Solid red line is a P type path; dashed line is S type path. α_1 and β_1 are the P- and S-velocities of the layer, α_2 and β_2 of the half-space.

$$V_{AP} = \Delta X/\Delta T = \alpha_1/\sin i \quad \text{or} \quad \Delta T = \Delta X \sin i/\alpha_1 \tag{3}$$

$$\Delta T = H\left[\sin^2 i/(\alpha_1 \cos i) - \text{sen j}\ \sin i/(\alpha_1 \cos j)\right] \tag{4}$$

Substituting (4) in (1) we have

$$T_{Ps} - T_P = H\left(\frac{\cos j}{\beta_1} - \frac{\cos i}{\alpha_1}\right) \tag{5}$$

H can be expressed in terms of the ray parameter, $p = (\sin i)/\alpha_1 = (\text{sen}\, j)/\beta_1 = 1/V_{AP}$

$$H = (T_{Ps} - T_P)/\left[\left(\beta_1^{-2} - p^2\right)^{1/2} - \left(\alpha_1^{-2} - p^2\right)^{1/2}\right] \tag{6}$$

as used by Zandt et al. (1995).

Therefore, to retrieve the sediment thickness (H) from the difference between Ps and P times, we need the P and S velocities of the sedimentary layer (which we will derive from the refraction experiment, as seen below), and the ray parameter (or apparent velocity V_{AP}), which depends on the earthquake location.

4. Receiver functions

Receiver functions (RF) are time series, obtained from seismograms of three-component stations, which typically contain mode conversions generated by steeply incident teleseismic P-waves which interact with subhorizontal structure beneath a seismometer (i.e., "receiver response"; Langston, 1979; Ammon, 1991a,b). Horizontal components rotated in the radial and transverse directions are deconvolved with the vertical component to produce, respectively, the radial and transverse receiver functions. The deconvolution eliminates the source signature, instrument response, and distant propagation effects (common to both vertical and horizontal components), and leaves basically only the converted S waves as if they were originated from a pulse of P wave incident on the base of the local structure (Langston, 1979; Owens et al., 1984; Ammon, 1991a,b). For 1D isotropic structures, the P-converted to S-wave appears only in the radial receiver function and the energy in the transverse receiver function should be theoretically zero.

The receiver function technique has been used successfully in Brazil for modeling deep structures such as the Moho discontinuity (Ammon et al., 1990; James et al., 1993; Assumpção et al., 2002, 2004; Krüger et al., 2002; França and Assumpção, 2004; Dourado et al., 2007; Julià et al., 2008), discontinuities of 410 km and 670 km in the upper mantle transition zone (Liu et al., 2003; Bianchi, 2009) as well as shallow features like sediment thickness, particularly in the Paraná basin (An and Assumpção, 2004; Costa et al., 2006; Silva et al., 2008; Zevallos et al., 2009).

In the case of large, deep structures, earthquakes with epicentral distances between 30° and 95° are used. For shallow structures in sedimentary basins, deep earthquakes (mainly from the subduction zone of the South American plate, at distances of 15°–20°) are used, which produce higher frequencies capable of resolving shallow discontinuities in sedimentary basin (Zevallos et al., 2009).

Here, we use the receiver function (RF) technique with small local events with epicentral distances 1–70 km and coda magnitudes 1.1–3.4 m_D, to best isolate the Ps conversion from the bottom of the sedimentary layer. Most of the best-located hypocentral depths, obtained with the closer 2005 network, range from 1 to 3 km. For epicentral distances between ~3 km (near stations) and ~20 km (far stations), the incidence angle at the base of the sedimentary layer (i_o in Figs. 4 and 5) varies from about 45° to 80°. Given the low velocities of the sedimentary layer, the average incidence angles within the layer (angles i and j in Fig. 5) are less than 30°. As explained above, very near the surface, the incidence angles are less than 10° because of even lower velocities of the surface layers right beneath the stations. This steep incidence justifies the use of the receiver function technique, as employed in teleseismic events.

When using receiver functions for teleseismic distances the plane-wave approximation is used to calculate synthetic RF and differential times. In our case, the plane-wave approximation is also valid as the high frequencies of the small earthquakes implies wavelengths around 200–300 m in the sedimentary layer for the direct P wave and about 100 m for the Ps conversion. These wavelengths are much smaller than the 3–70 km epicentral distances so that the plane-wave approximation used above to derive the travel times within a thin sedimentary layer are valid. This can be confirmed by exact calculations using a model with a 0.7 km thick surface layer over a half-space with P-wave velocities of 3.0 and 6.0 km/s, respectively. The Vp/Vs ratio of the surface layer is 2.5. For an epicentral distance of 3 km (typical of the closest events) and focal depth of 3 km, the exact Ps–P travel time difference is 0.361 s. The plane-wave approximation (Eq. (5) or (6)) yields a value of 0.371 s, less than 3% different. Considering that the sampling interval is 0.01s, this difference is negligible. Also, thinner layers or longer epicentral distances will produce even smaller errors.

The time-domain iterative deconvolution of Ligorría and Ammon (1999) was applied and the RFs deconvolution stability was assessed for each event by comparing the results of the observed and predicted radial component. To eliminate high frequency noise and scattering due to small heterogeneities, a low-pass Gaussian filter is traditionally used in the deconvolution. In our case we used a Gaussian width parameter $\alpha = 100$ (other values were tested and 100 was the best choice). This is equivalent to a cutoff frequency of 48 Hz, very close to Nyquist frequency (50 Hz). This means that the low-pass filter had no effect on our data, and that higher sampling rates could probably be used in the recordings. The size of the time window selected for the deconvolution varied according to the epicentral distance, usually including the whole P-wave train and stopping just before the S-wave. Finally, the receiver functions for each station were stacked to improve the signal-to-noise ratio and enhance the features of interest.

Following the methodology described above, receiver functions were determined for a set of 36 small, local earthquakes in Porto dos Gaúchos/MT: 26 of the 1998–2002 sequence (Table 1) and ten of the 2005 sequence (Table 2). We tried to select events located by the largest number of stations whenever possible. For some stations of the 1998–2002 deployment, however, we had to use events recorded by only two or three stations due to large epicentral distances (stations SJOB and JUAB) or short time of operation (FANB and TAGL). However, the receiver functions for each station from different events showed similar waveform pattern and no variations were observed in the Ps arrival time, as can be seen in Figs. 6–8 for JUAB (seven RFs), FJKB (nine RFs) and FPOR (four RFs) stations, respectively. The similarity of the RFs for different events shows that the deconvolution process really removed the source signature and produced a trace that depends only on the structure. The last trace in each figure is the stacked receiver function.

A record section with the stacked RF for each station is shown in Fig. 9. The largest peak is interpreted as the Ps conversion, except for stations JUAB and SJOB, both in granite outcrop outside the basin, which only show the direct P wave. The Ps–P time generally increases from north to south, being zero at JUAB and SJOB (i.e., the Ps is not observed; Fig. 6) and maximum at FPOR station (Fig. 8). Table 3 shows the Ps–P time differences measured in the stacked receiver functions for all 15 stations.

Table 1
Events of the 1998–2002 seismic sequence used for the receiver functions. Events are identified by date and origin time. Depths marked with "f" were fixed because of insufficient number of arrivals. Bold station codes indicate the stations with high signal-to-noise ratios used in the receiver function; the other stations were used only for location. Stations marked with (*) operated with analog smoked-paper seismographs. m_D is magnitude based on coda duration.

N°	Date dd/mm/yy	Time hh:mm	Latitude (°)	Longitude (°)	Deph (km)	m_D	Stations
01	04/04/1999	09:26	−11.603	−56.758	6.3	2.1	**BAT**, FJKB, JUAB
02	04/05/1999	03:26	−11.615	−56.757	5.0f	2.5	**JUAB**, FSJ(*), JOA(*)
03	07/05/1999	06:44	−11.590	−56.718	5.0f	3.3	**JUAB**, FSJ(*), JOA(*)
04	09/05/1999	14:24	−11.628	−56.766	6.2	3.0	**JUAB**, FSJ(*), JOA(*)
05	11/05/1999	20:15	−11.608	−56.765	6.4	3.4	**JUAB**, FSJ(*), JOA(*)
06	13/05/1999	16:41	−11.623	−56.741	5.0f	2.9	**JUAB, FJKB**, FSJ(*), JOA(*)
07	17/07/1999	15:18	−11.618	−56.752	7.3	2.1	**FANB**, FSJB, JOA(*)
08	26/07/1999	14:10	−11.600	−56.767	6.3	2.2	**FANB, JUAB**, FSJ(*), JOA(*)
09	07/08/1999	18:44	−11.639	−56.750	0.3	3.1	**JUAB**, FSJ(*), JOA(*)
10	30/01/2001	03:37	−11.601	−56.748	2.5	1.1	BAT, CMA, **FJKB**, FPOR, **FSJB**, JUAB
11	09/03/2001	01:06	−11.617	−56.780	0.0	1.9	**BAT**, CMA, FJKB, **FPOR**
12	11/06/2001	07:27	−11.623	−56.766	3.5	0.8	CMA, **FJKB**, FSJB, **OLAV**
13	21/06/2001	12:59	−11.620	−56.749	4.3	2.2	**CMA, FJKB, FSJB, OLAV**, JOA(*)
14	22/06/2001	05:58	−11.616	−56.751	3.5	2.4	**CMA, FJKB, FPOR, FSJB, OLAV**, JOA(*)
15	08/07/2001	03:26	−11.617	−56.767	3.5	1.9	**BAT**, CMA, FJKB, **FPOR**, FSJB
16	09/07/2001	23:16	−11.623	−56.766	3.4	1.8	**BAT, CMA**, FJKB, FPOR, FSJB
17	20/07/2001	05:38	−11.588	−56.722	1.9	1.8	BAT, **CMA, FJKB, FPOR, FSJB**
18	27/07/2001	00:22	−11.610	−56.715	2.6	2.0	BAT, **CMA, FJKB, FSJB**, JOA(*)
19	30/07/2001	19:43	−11.625	−56.739	0.1	1.9	FSJB, FJKB, **TAGL**
20	06/08/2001	11:55	−11.605	−56.769	4.7	2.4	FJKB, FSJB, **TAGL**, JOA(*)
21	31/10/2001	08:40	−11.623	−56.739	3.8	2.2	**CMA, FJKB, FSJB**, OLAV
22	01/11/2001	08:42	−11.622	−56.752	3.9	2.0	BAT, **CMA, FJKB, FSJB**, OLAV
23	25/06/2002	21:35	−11.595	−56.702	5.0f	2.1	FSJB, **SJOB**
24	26/06/2002	21:07	−11.590	−56.701	5.0f	2.1	FSJB, **SJOB**
25	09/12/2002	09:27	−11.590	−56.756	5.0f	1.1	CMA, **FBON**, JAKB, OLAB
26	09/12/2002	20:41	−11.618	−56.774	1.8	1.2	BAT, **CMA, FBON**, FPOR, **JAKB, OLAB**

Station PDRB is located in a granitic/gneissic outcrop in the middle of the sedimentary basin. In the RF section of Fig. 9, PDRB has the Ps conversion very close to the direct wave, indicating a very shallow average depth around that station as should be expected. Station BAT shows two peaks, one at 0.03 s and another at 0.16 s (Fig. 9). This station is also sited in hard rock but it is not clear if the outcrop is really a basement window or just a large boulder. Here we interpreted the Ps basement conversion as the peak arriving at 0.16 s. This interpretation is more consistent with the refraction data as shown in the next section.

5. Seismic refraction experiment

To help define the velocity structure in the PGSZ area a controlled source experiment was carried out in December 2002, with two explosions of 200 kg of dynamite, each fired in 40-m depth holes (stars 1 and 2 in Fig. 2). Shot 1 was close to station PDRB and was recorded by seven stations. Only stations of the aftershock studies were used to record the shots and no additional geophones were employed. Shot 2 was close to station JAKB and was recorded by nine stations. The first 10 m of the holes were filled with rubble in the first shot, and with concrete in the second one. For shot 1 basement rocks were found in the first 10 m, and for shot 2 only soil was found (Barros and Caixeta, 2003). The shot origin times were taken from a GPS clock directly connected to the explosion as well as by two sensors installed 153 m from shot point 1 (CH01) and 36 m from the shot point 2 (CH12).

The seismic sections in Fig. 10a (shot 1) and 10b (shot 2) show clear first arrivals at all stations. Fig. 11 shows the arrival times of both shots in the same plot. It can be seen that all arrivals from shot 2 (open circles in Fig. 11a) are later compared with shot 1 (closed square in Fig. 11a). This is because of the deep sedimentary layer beneath shot 2, compared with shot 1 (hard rock site).

A preliminary interpretation of the arrival times in Fig. 11a can be made as follows, using one layer over a half-space. The P-wave velocities of the sediments (direct wave) can be roughly estimated with the near geophone CH01 (153 m from shot point 1, Fig. 10a) and station JAKB (800 m from shot point 2, Fig. 10b) as 2.88 km/s and 2.84 km/s, respectively. The basement velocities (critically refracted wave from the half-space) are 6.18 (±0.04, std. error of the regression) km/s, for shot 1 between OLAB and SJOB, and 6.22 (±0.05) km/s for shot 2 between FBON and SJOB. A preliminary estimate of the sediment thickness using the velocities above ($\alpha_1 = 2.86$ km/s and $\alpha_2 = 6.20$ km/s) with an intercept of about 0.15 s (Fig. 10a) is $H = 0.24$ km.

The basement apparent velocities (6.18 and 6.22 km/s) are overestimated because the closer stations are in deeper parts of the basin (as shown by the RF section of Fig. 9) with larger delays

Table 2
Events of the 2005 seismic sequence used for the receiver functions. Bold station codes indicate the stations used for the RF study.

N°	Date dd/mm/year	Time hh:mm	Latitude (°)	Longitude (°)	Deph (km)	m_D	Stations
01	29/04/2005	13:09	−11.591	−56.735	0.5	1.8	**FBO2, FSJB, JAKB, OLA2, PDRB**
02	30/04/2005	23:04	−11.604	−56.735	0.1	1.7	**FBO2**, FSJB, **JAKB, OLA2**
03	03/05/2005	11:53	−11.595	−56.741	1.2	1.0	**FSJB, JAKB, OLA2**, PDRB
04	07/05/2005	10:13	−11.586	−56.732	0.5	1.7	**FSJB, JAKB, OLA2**, PDRB
05	07/05/2005	21:49	−11.607	−56.776	0.0	2.9	FBO2, **FSJB**, JAKB, **OLA2, PDRB**
06	08/05/2005	07:24	−11.601	−56.725	1.5	1.8	FSJB, **JAKB, OLA2**, PDRB
07	09/05/2005	19:17	−11.607	−56.775	0.0	1.1	**FBO2, FSJB**, JAKB, **OLA2**, PDRB
08	09/05/2005	19:45	−11.607	−56.727	0.0	1.4	**FBO2, FSJB**, JAKB, **OLA2**, PDRB
09	10/05/2005	15:26	−11.594	−56.727	1.4	2.2	**FBO2, FSJB**, JAKB, **OLA2**, PDRB
10	12/05/2005	15:34	−11.598	−56.751	0.4	1.7	**FBO2, FSJB, JAKB, OLA2, PDRB**

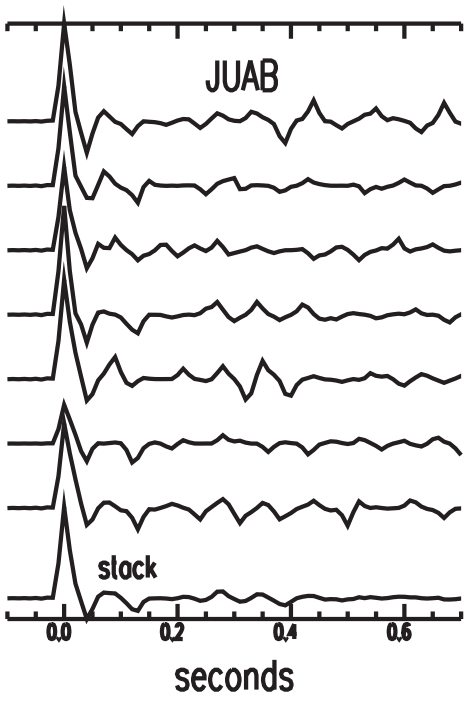

Fig. 6. Radial receiver functions for JUAB station located in the craton. The first seven traces (from top to bottom) are from Events 2, 3, 4, 5, 6, 8 and 9 of Table 1. The last trace is the averaged (stacked) receiver function. No Ps convertion is observed, only the direct P wave at 0.0 s.

compared with the more distant stations BAT and SJOB. Fig. 11a shows the expected arrival times from a reference model consisting of a sedimentary layer with P-wave velocity $\alpha_1 = 3.0$ km/s and thickness $H = 0.3$ km, overlying a basement half-space with P-wave velocity $\alpha_2 = 6.1$ km/s. The large dispersion in arrival times is due to

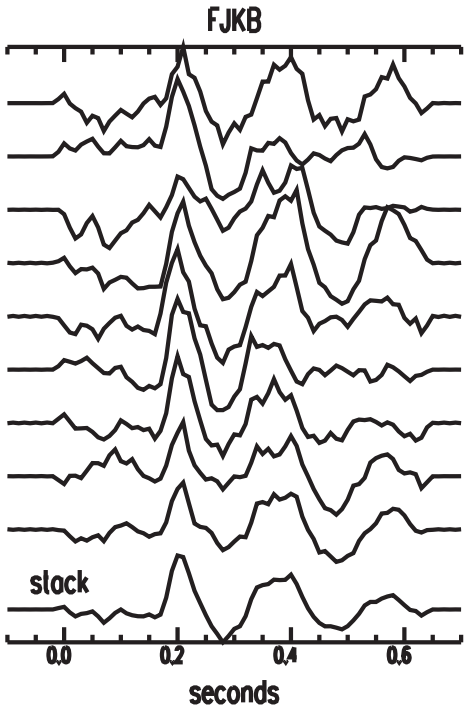

Fig. 7. Radial receiver functions for FJKB station located in the basin. First nine traces are from Events (from top to bottom) 6, 10, 12, 13, 14, 17, 18, 21 and 22 of Table 1. The last trace is the averaged (stacked) receiver function. The Ps phase is the coherent peak arriving at 0.20 s.

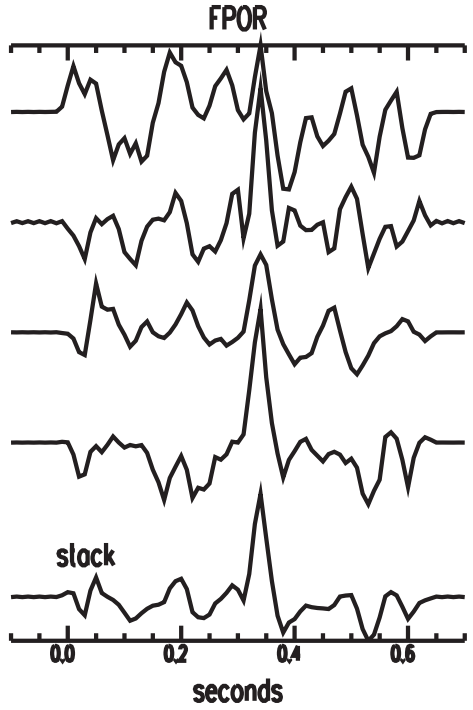

Fig. 8. Radial receiver functions for FPOR station located in the deepest part of the basin. The first four traces, from top to bottom, are from Events 11, 14, 15 and 17 of Table 1. The last trace is the average (stacked) receiver function. The Ps phase is the coherent peak arriving at 0.34 s.

the varying sedimentary thickness beneath the seismic stations. To properly interpret the refraction data, a correction in the P-wave arrival time must be applied to all stations based on the Ps–P time difference. The P-wave delay due to a sedimentary layer was normalized to a constant thickness (0.3 km in our case) and the corrected travel times are shown in Fig. 11b. However, the correction depends on the model velocities α_1 (sedimentary layer) and α_2 (basement). So, the joint interpretation of the refraction data with the Ps–P times (as shown in Fig. 11b) was the result of an iterative process.

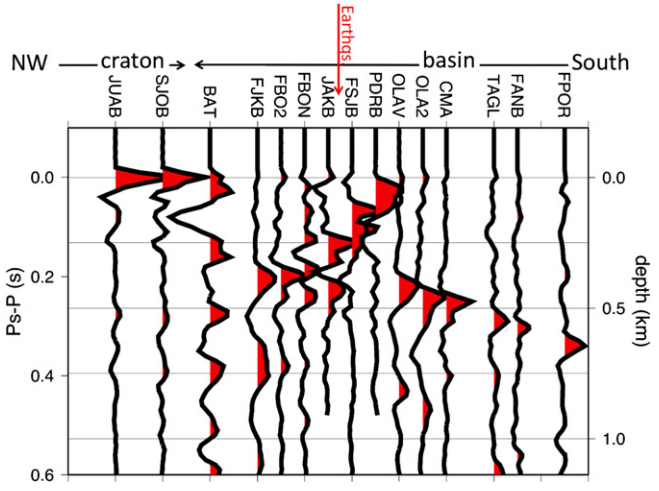

Fig. 9. Transect of all receiver function stacks. For stations JUAB and SJOB there are no phase conversions, as could be expected from their locations in the craton. Station PDRB is located on an isolated basement outcrop within the basin. All other stations are in the basin. Note that Ps–P increases toward the south. Depths were converted from the Ps–P times (see text). Stations were ordered along the white line shown in Fig. 12 (not to scale).

Table 3
Measured Ps–P time difference for all stations and corresponding basement depths (H) determined with Eq. (6). We used the P-wave velocity of the sedimentary layer $\alpha_1 = 3.0$ km/s and α_1/β_1 ratio = 2.5, according to the seismic refraction analysis. The apparent velocity was $p^{-1} = 6.4$ km/s (see text). Uncertainties in basement depths are about 20%.

N°	Station	Latitude (°)	Longitude (°)	Number of RFs	Ps–P (s)	H (m)
01	JUAB	−11.2163	−57.2577	07	0.00	0.0
02	SJOB	−11.4200	−57.0190	02	0.00	0.0
03	BAT	−11.4392	−56.7803	04	0.16	300
04	FJKB	−11.5553	−56.7950	09	0.20	380
05	FBO2	−11.5828	−56.7933	06	0.20	380
06	FSJB	−11.5750	−56.7088	15	0.07	130
07	FBON	−11.6000	−56.8150	02	0.19	360
08	JAKB	−11.6100	−56.7810	07	0.13	250
09	PDRB	−11.6122	−56.7297	03	0.025	50
10	OLAV/OLAB	−11.6272	−56.7267	04	0.22	420
11	OLA2	−11.6533	−56.7127	10	0.24	455
12	CMA	−11.6612	−56.8753	08	0.25	470
13	TAGL	−11.7252	−56.7310	02	0.29	550
14	FANB	−11.7387	−56.7498	02	0.30	570
15	FPOR	−11.7877	−56.7683	04	0.34	650

In a simple model with a uniform horizontal layer, with thickness H and P-wave velocity α_1, overlying a half-space with P velocity α_2 (as in Fig. 5), the P-wave time delay, a_p, beneath a station is given by:

$$a_p = H(\cos i)/\alpha_1, \quad \text{where } i = a\sin(\alpha_1/V_{AP}) \tag{7}$$

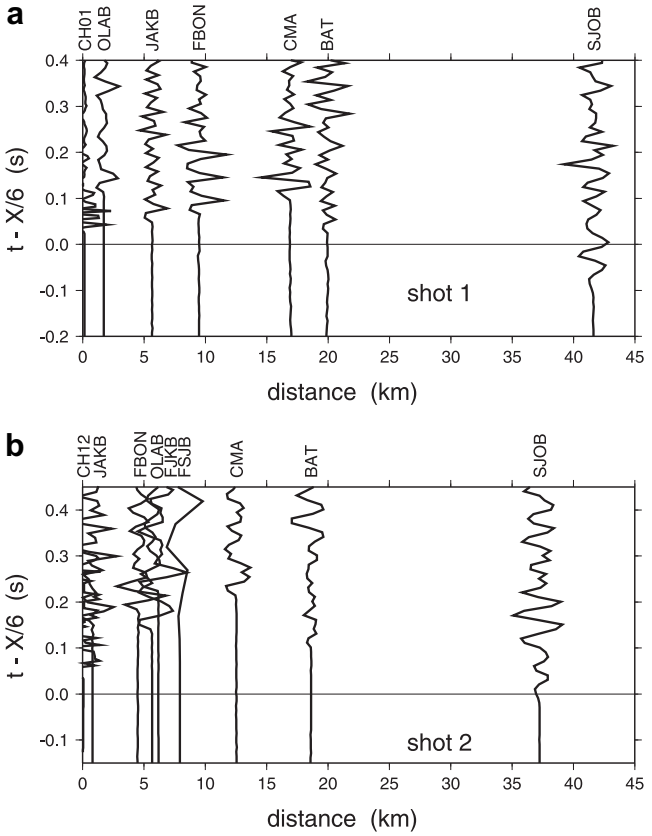

Fig. 10. Records of the seismic refraction study plotted with a reduced velocity of 6 km/s. Locations of shot points and stations are in Fig. 2. *a*) Shot point 1; CH01 is a geophone installed 153 m from the shot. *b*) Shot point 2; CH12 is a geophone installed 36 m from the shot; the low-resolution signal of FSJB station is due to the low sampling rate of only 20 Hz against 100 Hz used for all other stations.

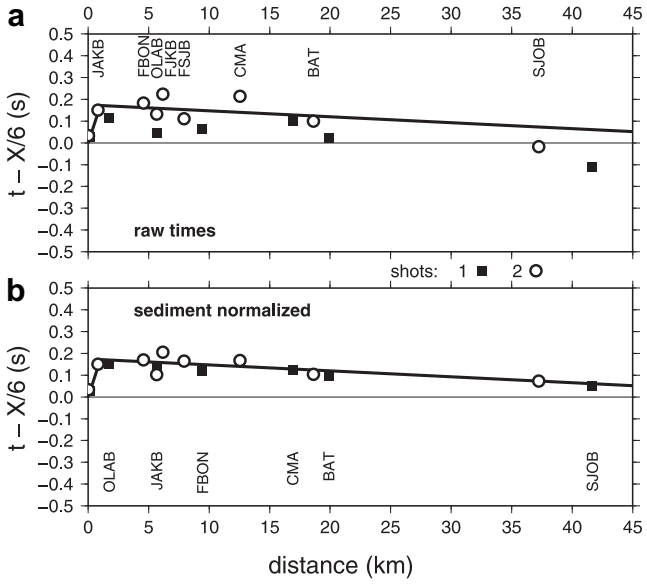

Fig. 11. P-wave time distance data for shot 1 (solid squares) and shot 2 (open circles) plotted with 6.0 km/s reduced velocity. The solid lines are the direct P-wave in the sedimentary layer and the critically refracted wave from the half-space calculated with the preferred model: $\alpha_1 = 3.0$ km/s, $\alpha_2 = 6.1$ km/s, $\alpha_1/\beta_1 = 2.5$, $H = 0.3$ km *a*) raw data, *b*) data corrected for variable sedimentary thickness and normalized to $H = 0.3$ km.

V_{AP} is the apparent velocity of the refracted ray, which is α_2 in the case of a critically refracted wave beneath a horizontal layer.

The Ps–P time difference, given by Eq. (6), is

$$T_{Ps} - T_P = H[(\cos j)/\beta_1 - (\cos i)/\alpha_1] \text{ where } j = a\sin(\beta_1/V_{AP}) \tag{8}$$

These equations give a relationship between the Ps–P time difference and the P-wave delay a_p:

$$T_{Ps} - T_P = [K(\cos j)/(\cos i) - 1]\cdot a_p \tag{9}$$

where $K = \alpha_1/\beta_1$ is the P-to-S velocity ratio in the sedimentary layer. Here we assume that the Ps phases from the local earthquakes were originated from P waves incident at the base of the sedimentary layer with a shallow angle, i.e., i_o in Fig. 5 is close to 90°, so that we can assume $V_{AP} \approx \alpha_2$ in Eq. (9). As explained above, the P waves from the local earthquakes hit the bottom of the sedimentary layer with an incidence angle i_o between 45° and 80°. Because the velocities of the sediments (α_1 and β_1) are much lower than V_{AP} the term $(\cos j)/(\cos i)$ in Eq. (9) is effectively close to 1, and the error introduced by assuming $V_{AP} = \alpha_2$ is less than 3%.

The travel time from the shot point to any station at a distance D can be given by

$$T_P = D/\alpha_2 + a_P(\text{shot}) + a_P(\text{station}) \tag{10}$$

The model parameters (α_1, K, α_2 and H) were varied by trial and error so that the travel times from the two shots were as consistent as possible, and the scatter of the travel times was reduced. The iteration process consists of: 1) Eq. (9) gives the P-wave time delay from the observed Ps–P for each station; 2) Eq. (7) gives the thicknesses for the shot points and stations, which are used to normalize all travel times to the model average thickness H; 3)

a reduced section is plotted to see how well the corrected data fit the trial model. All travel times were corrected using the Ps–P times in Table 3. Corrections included a station term as well as a term for the shot point, according to Eq. (10). For shot point 1 we used the same time delay as that of station PDRB, which was installed in the same outcrop. For shot-point 2 we used a time delay similar to the closest station JAKB.

We started the iteration process with parameters $H = 0.24$ km, $\alpha_1 = 2.9$ km/s, $\alpha_2 = 6.2$ km/s (given by the preliminary interpretation above), and $K = 2.0$. The corrections for the sediment are not sensitive to the basement velocity α_2, but depend mainly on α_1 and K. The best model, found by trial and error after a few iterations, was: $H = 0.3$ km, $\alpha_1 = 3.0$ km/s, $\alpha_2 = 6.1$ km/s, $K = 2.5$. Fig. 11b shows the resulting data and the fit to this best reference model. Not only the agreement between the two shots was improved, but the data scatter around the critical refraction from the basement was reduced.

The best model shows a large Vp/Vs ratio of 2.5, corresponding to a Poisson's ratio of 0.40. This is not uncommon in soil and unconsolidated sedimentary rocks. Barros et al. (2009) calculated the average Vp/Vs ratio for two different networks in PGSZ. The 1998 network, with an aperture of 70 km, included stations outside the basin such as JUAB (Fig. 1) and SJOB (Fig. 2) and had Vp/Vs = 1.71. The smaller network of 2005, closer to the epicentral area with stations only in the sedimentary basin, had an average Vp/Vs = 1.78 which shows the influence of the higher Vp/Vs ratio in the basin. In fact, for an average epicentral distance of 5 km (typical of the smaller 2005 network), the average Vp/Vs ratio for a ray path with 5 km in the basement (with $K = 1.71$) and 0.3 km in the sediments (with $K = 2.5$) is 1.786, quite consistent with the results of the Wadati diagram of Barros et al. (2009).

The large amplitudes of both the Ps and Sp converted phases (Fig. 3a and b) require a large velocity contrast in the sediment/basement interface. Therefore a high Poisson's ratio and low P velocity in the sediments should be expected. In addition, the P-wave velocity of the sediments ($\alpha_1 = 3.0$ km/s) must be lower than the S velocity of the basement ($\beta_2 = 6.1/1.71 = 3.57$ km/s) to ensure the existence of the refracted phase Sp.

6. Sediment thicknesses

The velocities of the best model above, obtained with the joint interpretation of the refraction data and the Ps–P times, were used to estimate the basin depth beneath each station using Eq. (6). In this case we chose an apparent velocity of 6.4 km/s (corresponding to an incidence angle beneath the bottom of the basement of $i_o = 70°$, more consistent with the hypocentral data). As explained earlier, variations of this apparent velocity affect the estimated depths by no more than 3%. The results are shown in Table 3. The average sedimentary thickness is 0.32 km, very similar to the thickness of the best 1D reference model.

Sensitivity tests with the final velocity model show that the basement velocity is well constrained at $\alpha_2 = 6.10 \pm 0.03$ km/s. Variations in the P-wave velocity of the sedimentary layer, α_1, cannot be larger than ±0.3 km/s and the *Vp*/*Vs* ratio, *K*, is well constrained at 2.5 ± 0.1. The effects on the depth values of the uncertainties in α_1 and *K* are 9% and 7%, respectively. We believe that the depth estimates in Table 3 are probably reliable to within 20–25%.

Fig. 12 shows a contour map of the basement depths using the values of Table 3 constrained with zero depth at the basin border. As already suggested by the RF section of Fig. 9, a basement high near the epicentral area (i.e., near stations PDRB and FSJB) can be seen superimposed in a general deepening of the basement toward the south (Fig. 12).

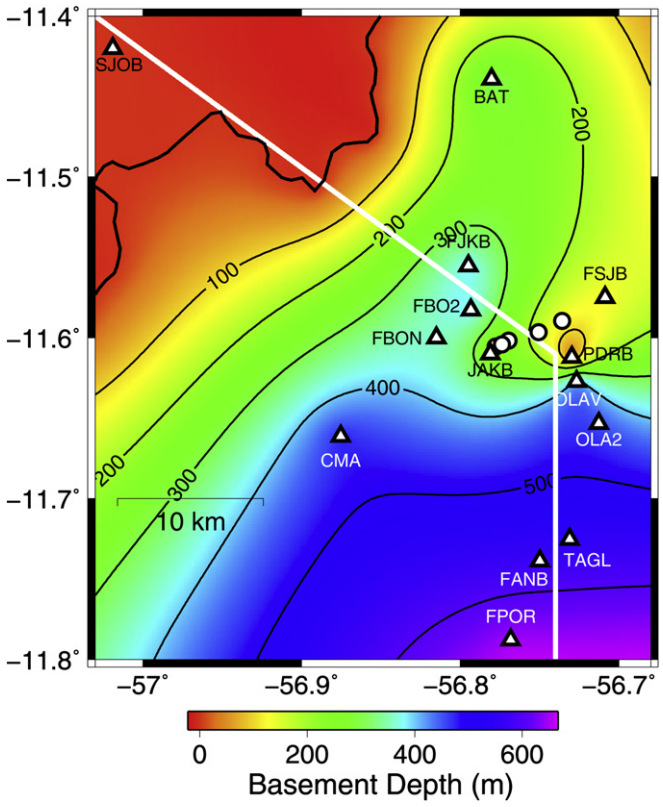

Fig. 12. Basement topography of the Parecis basin in the Porto dos Gaúchos study area, as obtained by receiver functions using local events recorded in the 15 stations indicated by the solid triangles. Color scale and contours are basin depth in meters not in km. Circles are the best-located five epicenters of the 2005 seismic sequence. The thick solid line is the limit between the granitic/gneissic craton outcrop and the basin sediments. The white line is the transect used to display the Receiver Functions in Fig. 9.

7. Discussion

The proposed velocity model and sediment thicknesses for the Parecis basin in the PGSZ were obtained by combining data from a controlled source experiment and P-to-S conversions from local earthquakes. Ps–P times are very consistent for each station (see Figs. 7 and 8). The basement high observed *in-situ* at shot-point 1 was clearly detected by the receiver functions of the station PDRB (which is sited in a granite/gneiss outcrop) as seen in the section of Fig. 9. This confirms that the Ps phase was correctly interpreted as a P-to-S conversion in the basement/sediments interface. The large pulse width in PDRB station (Fig. 9) could be due to the sharp variation in the relief of the basement. This can influence the converted phases as our methodology assumes a homogeneous layered medium.

The large differences between the Braga and Siqueira (1996) regional model of basement depths (Fig. 2) and the model proposed here (Fig. 12) are related to the different scales and methodologies. Braga and Siqueira (1996) modeled regional variations of Bouguer gravity anomalies over the whole Parecis Basin as due to basement topography only. The highs and lows in the Bouguer gravity anomalies were interpreted as basement highs and lows. Besides, the model of Braga and Siqueira (1996) was constrained by sparse seismic and well data located far from our study area, mainly near the Pimenta Bueno graben in the southern part of the Parecis basin. As no independent depth control was used near our study area, their estimated depths have no local meaning,

except to indicate a trend of lower gravity toward the Xingu and Caiabis graben systems to the north.

Our model shows more detailed local structures in a small area around the Porto dos Gauchos Seismic Zone. Contrary to the gravity-derived model, our basement depth tends to increase to the south, away from the northern border of the Parecis basin. We conclude that the decrease in gravity toward the north (as used by Braga and Siqueira, 1996) must be caused by variations of deeper crustal structure, such as variations in crustal thickness in the Parecis basin.

Near the epicentral area (Fig. 12) a large difference of 0.4 km in basement depth was found between stations PDRB and OLAV, which are only 1.7 km apart. This shows that there is an important structure in the basement, such as the border fault of a buried graben, perhaps. Stations JAKB, PDRB and FSJB show shallower basement compared to other stations to the north and to the south (Fig. 12). This suggests a basement high oriented approximately in the ENE–WSW direction, roughly parallel to the PGSZ, as shown by the five best-located epicenters of the 2005 sequence (Fig. 12). It is interesting to note that in the PGSZ, aeromagnetic anomalies show lineaments also in the ENE–WSW direction (Fig. 4 of Barros et al., 2009).

The 1998 and 2005 earthquake sequences both occurred in a single N60°E trending fault system about 6 km long (Barros et al., 2009) roughly consistent with the continuation of a geological fault mapped in the nearby Caiabis graben by Leite and Saes (2003) (see Fig. 1). Hypocentral depths ranged from a few hundred meters to about 3 km or more (Barros et al., 2009). It is likely that the basement high detected with the receiver functions is also related to the seismogenesis of the PGSZ. The few available data on the basement topography (Table 3 and Fig. 12), however, do not allow a detailed geometrical description of that basement high, and so we cannot present a detailed seismotectonic explanation for the 1998 and 2005 earthquakes. Nevertheless, this important basement structure clearly deserves further studies in the future with other geophysical surveys and more dense seismic lines. Schulte and Mooney (2005) showed that about 27% of all continental intraplate earthquakes are related to ancient interior rifts or continental margins. Therefore more detailed studies of the Parecis basement relief should be encouraged to see if the basement step detected in this study could be the trace of an ancient buried graben reactivated under the present stresses.

8. Conclusions

The use of receiver function with small local earthquakes proved to be very useful in determining sediment thicknesses in the Parecis basin. The high velocity contrast between basement and sediments favors the generation of clear converted phases in the receiver function (Ps) and also in the vertical component (Sp phase). This application could be extended to other seismic areas in sedimentary basins, where large velocity contrasts between sediments and basement rocks are present.

The combined use of a controlled seismic experiment and the Ps–P times allowed determination of a velocity model for the PGSZ and sediment thicknesses beneath each station. The map of basement topography revealed an important structural high, maybe trending in the ENE–WSW direction. We propose that this structural feature is part of a larger system of ENE–WSW oriented faults that could be related with the 1998 and 2005 earthquake sequences. The present study did not have enough stations for a detailed geometrical characterization of this basement feature, but clearly indicates the relevance of further studies with other geophysical surveys (such as local gravity and magnetics) and more dense seismic lines to better understand the important Porto dos Gaúchos Seismic Zone.

Acknowledgments

Many people contributed with hard work to deploy the stations and collect data from remote areas in Porto dos Gaúchos, especially Daniel Caixeta, Darlan Portela, Isaú Gomes, Juraci Carvalho and Daniel Linhares. We thank the geology students who worked on the data preparation (Ranielle Paz, Vinícius Ferreira). We also thank Edna Leony, Kate Sousa, and Luzia de Freitas from the Seismological Observatory staff that in different ways helped us in this work. Finally we thank the farmers Selso Rosato, Olavo Webber, José Kavichioli and Jackson for permission to deploy stations in their lands and the station operators José Aparecido and Oscar de Almeida. We would like to thank L.P.S. Braga for the basement topography data used in Figs. 1 and 2. We thank Andy Frassetto, two anonymous reviewers and the editors who made valuable suggestions to improve the paper.

References

Almeida, F.F.M., Neves, B.B.B., Carneiro, C.D.R., 2000. The origin and evolution of the South American Platform. Earth-Sci. Rev. 50, 77–111.

Ammon, C.J., 1991a. The isolation of receiver effects from teleseismic p waveforms. Bull. Seismological Soc. Am 81 (6), 2504–2510.

Ammon, C.J., 1991b. An Overview of the Receiver-function Analysis. http://eqseis.geosc.psu.edu/.

Ammon, C.J., Randall, G.E., Zandt, G., 1990. On the nonuniqueness of receiver function inversion. J. Geophys. Res. 95 (B10), 15303–15318.

An, M., Assumpção, M., 2004. Basement depth in the Paraná Basin with high frequency receiver functions. In: I Simpósio Regional. Sociedade Brasileira de Geofísica, São Paulo, Brazil.

Assumpção, M., James, D.E., Snoke, A., 2002. Crustal thickness in SE Brazilian Shield by receiver function analysis: implications for isostatic compensation. J. Geophys. Res. 616 (107), 2006. doi:10.1029/2001JB000422.

Assumpção, M., An, M., Bianchi, M., França, G.S., Rocha, M., Barbosa, J.R., Berrocal, J., 2004. Seismic studies of the Brasília fold belt at the western border of the São Francisco craton, central Brazil, using receiver function, surface wave dispersion, and teleseismic tomography. Tectonophysics 388, 173–185 (Amsterdam), Holand.

Barros, L.V., 2010. Seismicity, tectonic stresses and crustal structure in the Porto dos Gaúchos seismic zone, MT. PhD Thesis (in Portuguese), Institute of Geosciences, University of Brasilia, Brasília, Brazil.

Barros, L.V., Caixeta, D.F. 2003. Unidimensional multilayer velocity model for Porto dos Gaúchos/MT. In: 8 Int. Cong. of SBGf, September 14–18, 6 pp.

Barros, L.V., Assumpção, M., Quintero, R., Caixeta, D.F., 2009. The intraplate Porto dos Gaúchos seismic zone in the Amazon craton – Brazil. Tectonophysics 469, 37–47.

Barros, L.V., Assumpção, M., Quintero, R., Ferreira, V.M., 2011. Coda wave attenuation in the Parecis basin, Amazonian craton e Brazil: sensitivity to basement depths. J. Seismol 15, 391–409. doi:10.1007/s10950-011-9231-1.

Bianchi, M.B., 2009. Variations in the crustal, lithosphere and mantle structure for South American Platform using P- and S-waves receiver functions. PhD Thesis (in portuguese), Instituto de Astronomia, Geofísica e Ciências Atmosférica – Universidade de São Paulo, 133 pp.

Braga, L.F.S., Siqueira, L.P. 1996. Three dimensional gravity modelling of the basement topography beneath Parecis Basin, Brazil, constrained by DBNM, spectral estimates of depth to magnetic sources. In: 5th Latin Amer. Petr. Cong. Rio de Janeiro, Brazil.

Costa, T.N., Assumpção, M., Barbosa, J.R., 2006. Estudo de espessura sedimentar na Bacia do Paraná com função do receptor de alta freqüência. In: II Regional Geophysical Symposium Braz. Geophys. Soc. Natal, (extended abstract).

Dourado, J.C., Assumpção, M., Malagutti-Filho, W., Bianchi, M.B., 2007. Crustal features determined by azimuthal analysis of receiver functions in the area of the Rio Claro seismological station, RCLB. (in Portuguese). Rev. Bras. de Geofísica 25, 399–411.

França, G.S.L.A., Assumpção, M., 2004. Crustal structure of the fold belt, SE Brazil, derived from receiver functions. J. South Am. Earth Sci. 16, 743–758.

James, D.E., Assumpção, M., Snoke, A., Ribotta, L.C., Kuehnel, R., 1993. Seismic studies of continental lithosphere beneath SE Brazil. Acad. Bras. Cienc. 65 (Suppl. 2), 227–250.

Julià, J., Assumpção, M., Rocha, M., 2008. Deep crustal structure of the Paraná basin from receiver functions and Rayleigh-waves dispersion: evidence from a fragmented cratonic root. J Geophys Res doi:10.10x29/200/JB005374.

Krüger, F., Scherbaum, F., Rosa, J.W.C., Kind, R., Zetsche, F., Höhne, J., 2002. Crustal and upper mantle structure in the Amazon (Brazil) determined with broad band mobile stations. J. Geophys. Res. 107 (B10), 2265.

Langston, C.A., 1979. Structure under Mount Rainier, Washington, inferred from teleseismic body waves. J. Geophys. Res. 84, 4749–4762.

Leite, J.A., Saes, G.S., 2003. Geocronologia Pb/Pb de zircões detríticos e análise estratigráfica das coberturas sedimentares Proterozóicas do sudeste do Cráton Amazônico, vol. 3. Rev. do Instituto de Geociências da USP, São Paulo, pp. 113–127.

Ligorría, J.P., Ammon, C.J., 1999. Iterative deconvolution and receiver function estimation. Bull. Seism. Soc. Am. 89, 1395–1400.
Liu, K.H., Gao, S.S., Silver, P.G., Zang, Y., 2003. Mantle layering across central South America. J. Geophys. Res. 108 (B11), 2510.
Owens, T.J., Zandt, G., Taylor, S.R., 1984. Seismic evidence for an ancient rift beneath the Cumberland Plateau, Tennessee: a detailed analysis of broadband teleseismic P waveforms. J. Geophys. Res. 89, 7783–7795.
Schulte, S.M., Mooney, W.D., 2005. An updated global earthquake catalogue for stable continental regions: reassessing the correlation with ancient rifts. Geophys. J. Int. 161, 707–721.
Silva, J.A., Souza, L.M., Assumpção, M., 2008. Espessura e velocidade das camadas sedimentares na borda nordeste da bacia do Paraná utilizando telessismos da região Andina e sismos locais. In: Rio Oil & Gás 2008, IBP1812_08. Rio de Janeiro, 15–18 de setembro de 2008.
Siqueira, L.P., 1989. Bacia dos Parecis. Geociências PETROBRAS 3 (112), 3–16.
Tassinari, C.C.G., Bittencourt, J.S., Geraldes, M.C., Macambira, M.J.B., Lafon, J.M., et al., 2000. The Amazonian craton. In: Cordani (Ed.), Tectonic Evolution of South America. 31st Int. Geol. Congr, Rio de Janeiro, pp. 41–95.
Zandt, G., Myers, S.C., Wallace, T.C., 1995. Crust and mantle structure across the basin and range – Colorado plateau at 37°N latitude and implications for Cenozoic extensional mechanism. J. Geophys. Res. 100, 10.529–10.548.
Zevallos, I., Assumpção, M., Padilha, A.L., 2009. Inversion of teleseismic receiver function and magnetotelluric sounding to determine basement depth in the Paraná Basin, SE Brazil. J. Appl. Geophys. 68, 231–242.